Original Article

Institution of MECHANICAL ENGINEERS
Journal of AEROSPACE ENGINEERING

Identification for a reentry vehicle via Levy flight-based pigeon-inspired optimization

Proc IMechE Part G: J Aerospace Engineering
2018, Vol. 232(4) 626–637

DOI: 10.1177/0954410016682274
journals.sagepub.com/home/pig
SAGE

Daifeng Zhang and Haibin Duan

Abstract

Reentry vehicles are valuable both in the military domain and scientific research. However, the high-order nonlinearity of mathematical models is always a bottleneck for reentry study. One of the reasons is the difficulty to measure the involved aerodynamic parameters. Therefore, parameter identification is a crucial issue in modeling and controller design for reentry vehicles. This paper mainly focuses on the identification approach for aerodynamic parameters of an existing reentry vehicle. Wind field turbulences are modeled to imitate the real flight scenarios. A novel bio-inspired optimization algorithm is proposed to solve this problem. Our proposed method stems from the pigeon-inspired optimization, which is an effective swarm intelligence optimizer utilized in many research areas. Typical characteristics of Levy flight are drawn on to improve the global accuracy of the new algorithm. Finally, comparative experiments with some homogenous methods are conducted to verify the expected performances of our identification algorithm.

Keywords

Reentry vehicle, parameter identification, wind turbulences, pigeon-inspired optimization, Levy flight

Date received: 26 September 2016; accepted: 10 November 2016

Introduction

Reentry vehicle is a family of advanced hypersonic aircrafts with much research value in both military and civil fields, whose velocity is five times greater than the Mach number.[1] Reentry phase is a crucial stage for the flight safety of reentry vehicles in hypersonic environments. During the reentry phase, reentry vehicles are always subject to complex risks such as strong wind shears, high-frequency vibration, and aerodynamic coupling, thus leading to high challenges for reentry modeling and controller design. For example, in terms of reentry modeling, the aerodynamic forces and moments of reentry vehicles are always nonlinear and time-variant thus making the token aerodynamic parameters difficult to determine. Besides, the precise estimation of aerodynamic parameters is of significance for the deployment and execution of specific reentry tasks such as attitude control and trajectory planning. To guarantee the stability and safety in hypersonic flight, reentry controllers always employ advanced methods such as adaptive neural network,[2] back-stepping control,[3,4] robust fuzzy control,[5] etc. However, most of them require accurate and stable estimation of flight state variables including aerodynamic parameters. Therefore, it is necessary to take into consideration the identification and determination of the aerodynamic parameters for reentry research.

As for the modeling of reentry vehicles, some breakthroughs sprang up in recent years. Air Force Research Laboratory (AFRL) and National Aeronautics and Space Administration (NASA) have executed a large number of studies on the foundation of aerodynamic data base for reentry vehicles. Oppenheimer et al.[6] used the Piston Theory to calculate the aerodynamic forces of hypersonic motion in reentry phase and presented a flexible reentry model. Researchers from NASA Langley Research Center[7] introduced the Winged-Cone aerodynamic model for hypersonic vehicles. This model was developed via the computational fluid dynamics (CFD) analysis codes conducted at NASA Langley and Rockwell International, which has been used in many hypersonic researches such as trajectory optimization, stability augmentation, etc. In the Winged-Cone model, the aerodynamic coefficients

Bio-inspired Autonomous Flight Systems (BAFS) Research Group, Science and Technology on Aircraft Control Laboratory, School of Automation Science and Electrical Engineering, Beihang University, Beijing, PR China

Corresponding author:
Haibin Duan, Bio-inspired Autonomous Flight Systems (BAFS) Research Group, Science and Technology on Aircraft Control Laboratory, School of Automation Science and Electrical Engineering, Beihang University, Beijing 100083, PR China.
Email: hbduan@buaa.edu.cn

were described as functions of Mach number, attack angle, and control surface deflections. Keshmiri et al.[8] created a group of fitted five-order polynomials based on the combination of the Winged-Cone and wind tunnel model to give a summary and guidance for reentry modeling. Klock et al.[9] applied model reduction techniques to research the aerodynamic, thermodynamic, and structural dynamic system evolution and couplings on a hypersonic vehicle. Prandtl–Meyer expansion and Piston Theory were combined to create an approximate flow solution, and free vibration mode shapes (FVMS) were used to generalize the low-order structural dynamics and motion equations. Meanwhile, as inevitable turbulence sources, wind disturbances are necessarily considered in the reentry modeling. Liang et al.[10] used the Reynolds-averaged Navier–Stokes (RANS) transition/turbulence model to simulate the hypersonic flow transition. The rational effects of compressibility, crossflow, and flow separation were involved and the model was validated with a number of available experiments on boundary layer transition. Dryden computational model[11–13] is widely used in wind field modeling, which is approximate to the realistic wind fields in both low and high altitude, and is proved suitable for hypersonic wind fields.

However, because the reentry models always include the hard-to-measure aerodynamic parameters, the relevant identification is a necessary issue for reentry research. Time domain-based identification methods are preferred for reentry models on account of its facility and feasibility. Vitale et al.[14] presented the unscented Kalman filter (UKF) approach to estimate the lateral-directional aerodynamic model of a reentry vehicle in subsonic, transonic, and supersonic regimes. This method performed reliable estimation and was used to supplement the refinement of the flying test bed (FTB) aerodynamic model. Hu et al.[15] proposed a recursive maximum likelihood (RML) method to online estimate the uncertain hypersonic aerodynamic parameters. The interior-point algorithm is applied to optimize the boundaries of unknown parameters and assist the basic RML to keep the identification results in a reasonable range. Other common approaches in time domain include extended Kalman filter (EKF)[16] and least squares (LS) method,[17] etc. However, most of them are based on the analytical gradient accuracy of objective function, and concerned to be limited for the reentry models under strong turbulences for the reason that the large span of speed and highly exterior uncertainty make it restrained to obtain precise gradients. Swarm intelligence optimizers[18] are effective approaches on complex model identification due to its independence of objective model. These bio-inspired algorithms include particle swarm optimization[19] (PSO), differential evolution[20] (DE), artificial bee colony[21,22] (ABC), etc. Besides, pigeon-inspired optimization[23–29] (PIO) is a novel method, which has been proved more efficient than the former homogenous methods in some specific cases.

Table 1. Geometric parameters of reentry vehicle.

Reference area (ft^2)	3603.00
Span (ft)	60.00
Mean aerodynamic chord (ft)	80.00
Moment reference center (ft)	124.01
Vehicle weight with engine closed (lb)	140,000.00

The remainder of this paper will be arranged as follows. Firstly, the nonlinear model of a specific reentry vehicle with certain wind field disturbances is presented. Then, a novel Levy flight-based bio-inspired algorithm is introduced and analyzed next. The parameter identification process via the proposed approach is discussed and comparative experiments as well as result analysis are conducted in later sections. Finally, the conclusion of this paper is given in final section.

Modeling for reentry vehicle with wind field

As is mentioned above, some certain mathematical models for reentry vehicles are available to our research. Here, we adopt the Winged-Cone model raised by NASA Langley as the parameter database of the aerodynamic forces and moments. Some fixed geometric parameters of the specific reentry vehicle in this paper are listed in Table 1 and the geometry configuration with some necessary coordinate systems are given in Figure 1.

Motion equations of reentry vehicle

Before introducing the Winged-Cone model, we first present some basic coordinate frames and relevant aerodynamic angles. As shown in Figure 1, the frame with suffix b represents the body frame as axis x is inside the body symmetry plane, while other frames with suffix a and k denote the velocity and flight path coordinates respectively as axis x is parallel to the flight velocity. Moreover, the frame with suffix g is seen as the local Cartesian coordinate system (ENU coordinates). The angles α and β (degree) represent the attack and side-slip angle, which execute the rotational transform between body and velocity frames, whereas μ, χ, and γ (rad) are flight path angles, which indicate the transition between the ENU and flight path frames. Besides, the variables p, q, r (rad/s) denote the angular rates along body frame (roll, pitch, and yaw rates). Hence, the motion equations are easily obtained by composition of forces and moments as well as transformation matrices between basic frames. To simplify the derivation process, we directly give the following motion

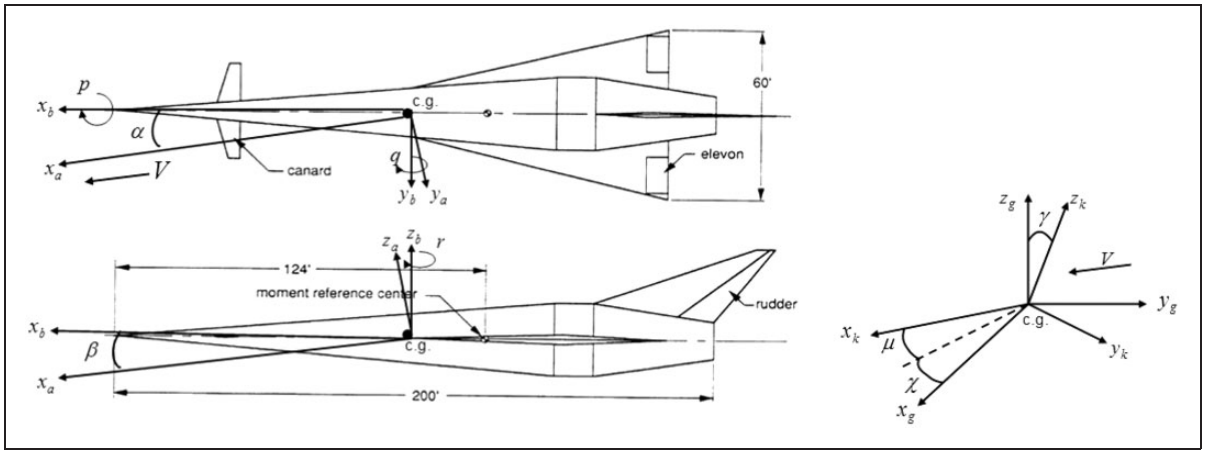

Figure 1. Geometry configuration with basic coordinate systems.

equations of reentry vehicles

$$\begin{aligned}
\dot{V}_a &= \frac{1}{M}(-D - Mg\sin\gamma)\\
\dot{\chi} &= \frac{1}{MV_a\cos\gamma}(Y + Mg\sin\mu\cos\gamma)\\
\dot{\gamma} &= \frac{1}{MV_a}(L - Mg\cos\mu\cos\gamma)\\
\dot{\alpha} &= q - \tan\beta(p\cos\alpha + r\sin\alpha)\\
&\quad + \frac{1}{MV_a\cos\beta}(-L + Mg\cos\gamma\cos\mu)\\
\dot{\beta} &= -r\cos\alpha + p\sin\alpha\\
&\quad + \frac{1}{MV_a}(Y\cos\beta + Mg\cos\gamma\sin\mu)\\
\dot{\mu} &= \sec\beta(p\cos\alpha + r\sin\alpha)\\
&\quad + \frac{L}{MV_a}(\tan\beta + \tan\gamma\sin\mu)\\
&\quad - \frac{g}{V_a}\tan\beta\cos\gamma\cos\mu\\
\dot{p} &= \frac{(I_y - I_z)qr}{I_x} + \frac{1}{I_x}l\\
\dot{q} &= \frac{I_z - I_x}{I_y}pr + \frac{1}{I_y}m\\
\dot{r} &= \frac{I_x - I_y}{I_z}pq + \frac{1}{I_z}n
\end{aligned} \tag{1}$$

where D, L, and Y (lb) denote the total drag, lift, and side forces, and l, m, and n (lb · ft) is the total moments along three body axis respectively. V_a (ft/s) defines the airspeed value. Note that the moment reference center is different from the center of gravity or body frame center (c.g.), therefore some transformation process between moments is necessary when discussing the aerodynamic model. I_x, I_y, and I_z (lb · ft · s^2) represent the inertia moments along body frame.

According to the Winged-Cone model, the aircraft weight M (lb) is changeable with fuel flow. In this paper, we assume a constant weight due to the slight depletion of oil during the short motion period, and the reaction control system[30] (RCS) is also invalid. The total forces and moments above are strongly relevant to aerodynamic parameters, hence the next content will introduce the Winged-Cone database.

Winged-cone model

The computation of the total forces and moments of reentry vehicles is of the same form as the fixed-wing aircraft, which is shown in the following equations

$$\begin{aligned}
L &= C_L S_{ref}\bar{q}\\
D &= C_D S_{ref}\bar{q}\\
Y &= C_Y S_{ref}\bar{q}\\
l &= C_l S_{ref}\bar{q}b\\
m &= C_m S_{ref}\bar{q}c - x_{cg}Z\\
n &= C_n S_{ref}\bar{q}b + x_{cg}Y
\end{aligned} \tag{2}$$

where S_{ref}(ft^2) is the wing area of the reentry vehicle, $\bar{q} = \rho V_a^2/2$ (lb/ft^2) is the dynamic pressure, and ρ(kg/ft^3) represents the density of atmosphere. C_L etc. denote the relative force coefficients, and respectively C_l etc. represent the moment coefficients. Define x_{cg} (ft) is the longitudinal distance from the moment reference center to c.g., hence according to Figure 1, the moments m and n are complemented with coupling moments to keep equilibrium and $Z = -D\sin\alpha - L\cos\alpha$ denotes the composition of the lift and drag component forces along z body axis.

According to the winged-cone model, force and moment coefficients can be divided into several increments as follows

$$\begin{aligned}
C_L &= C_{L\alpha} + C_{L\delta_a} + C_{L\delta_e}\\
C_D &= C_{D\alpha} + C_{D\delta_a} + C_{D\delta_e} + C_{D\delta_r}\\
C_Y &= C_{Y_\beta}\cdot\beta + C_{Y\delta_a} + C_{Y\delta_e} + C_{Y\delta_r}
\end{aligned}$$

$$
\begin{aligned}
C_l &= C_{l_\beta}\cdot\beta + C_{l\delta_a} + C_{l\delta_e} + C_{l\delta_r} \\
&\quad + C_{l_p}\left(\frac{pb}{2V_a}\right) + C_{l_r}\left(\frac{rb}{2V_a}\right) \\
C_m &= C_{m\alpha} + C_{m\delta_a} + C_{m\delta_e} + C_{m\delta_r} + C_{m_q}\left(\frac{qc}{2V_a}\right) \\
C_n &= C_{n_\beta}\cdot\beta + C_{n\delta_a} + C_{n\delta_e} + C_{n\delta_r} \\
&\quad + C_{n_p}\left(\frac{pb}{2V_a}\right) + C_{n_r}\left(\frac{rb}{2V_a}\right)
\end{aligned} \tag{3}
$$

where δ_a, δ_e, δ_r (degree) denote the aileron, elevator, and rudder deflections as system inputs. The control surface of canard shown in Figure 1 is ignored in this model due to its little influence on the aerodynamics during reentry phase. Respectively b and c are the lateral and longitudinal reference span. The items with suffix L, D, Y denote the force coefficient increments, whereas others with suffix l, m, and n represent the moment coefficient increments. Besides, the items with suffix α and δ can be expressed as polynomials of attack and control surfaces. Others with two-stage indexes represent the derivatives of relative states. Note that the angular rates are normalized in these equations.

The increments of the aerodynamic coefficients are functions of Mach number, attack angle and control deflections in the form of relation curves;[7] however, no regular expressions that summarize those properties are developed recently. Keshmiri et al.[8] combined the Winged-Cone model with the wind tunnel data and presented a group of five-order polynomials to fit this model precisely via interpolation and extrapolation. However, most scaling parameters in these polynomials are unknown, and many of them are too small to estimate precisely. Due to the parameters associated with high-order items are far smaller than those with low-order ones, we extract the basic and first-order items of each polynomial and reduce the order of Winged-Cone model to facilitate this research.

Given the prerequisites above, we extract the simplified winged-cone polynomials. For example, the lift coefficient increment for attack angle and elevator deflection are represented as

$$
\begin{aligned}
C_{L\alpha} &= a_{1,1} + a_{1,2}\alpha + a_{1,3}M_a + o(\alpha, M_a) \\
C_{L\delta_a} &= a_{2,1}\alpha + a_{2,2}M_a + a_{2,3}\delta_a + o(\alpha, M_a, \delta_a)
\end{aligned} \tag{4}
$$

where $a_{i,j}$ are the polynomial parameters to be identified and $o(\alpha, M_a)$, $o(\alpha, M_a, \delta_a)$ are high-order items associated with relative states. Other aerodynamic coefficient increments can be expressed as similar format respectively.

Modeling of wind field disturbances

Reentry vehicles usually fly 20 km above the earth where stratosphere and mesosphere must be considered. Strong wind shears and turbulences always occur in this area which cannot be ignored. NASA Marshall Space Flight Center[11] has formed and evaluated the wind field model in both low and high altitude, and presented a few specific criteria guidelines to cope with various situations. Hence, we prefer to adopt this model to imitate the realistic wind field in reentry phase. Normally, the wind field includes two kinds of components: gusts and shears. The gusts can be described as[12]

$$
\begin{cases}
\boldsymbol{V}_G = 0 & t < 0 \\
\boldsymbol{V}_G = \frac{V_{Gm}}{2}[1 - \cos(\pi t/t_m)] & 0 \leqslant t \leqslant t_m \\
\boldsymbol{V}_G = \frac{V_{Gm}}{2} & t > t_m
\end{cases} \tag{5}
$$

where $\boldsymbol{V}_G = (u_G,\ v_G,\ w_G)$ and $\boldsymbol{V}_{Gm}$ are the current and maximum gust wind speed vector and no wind gradient occurs when $t > t_m$. As for wind shears, the speed vector is given as $\boldsymbol{V}_S = \bar{\boldsymbol{V}}_S + \tilde{\boldsymbol{V}}_S$, where $\bar{\boldsymbol{V}}_S = (\bar{u}_S, \bar{v}_S, \bar{w}_S)$ is a constant mean value and $\tilde{\boldsymbol{V}}_S = (\tilde{u}_S, \tilde{v}_S, \tilde{w}_S)$ represents the random disturbance vector. The random vectors can be expressed as Dryden computational model as in Figure 2.[11–13]

WNG denotes Gauss white noise. Six transfer functions in the shape of filters are used to generate the random vectors and part of wind shear gradients v_x, v_z, w_x, while other gradients are near zero. According to Du et al.,[31] the aerodynamics of total wind field can be described as

$$
\dot{\boldsymbol{V}}_W = \begin{bmatrix} \dot{u}_W \\ \dot{v}_W \\ \dot{w}_W \end{bmatrix} = \begin{bmatrix} u_x\cdot(V_a + u_W) + u_y\cdot v_W + u_z\cdot w_W \\ v_x\cdot(V_a + u_W) + v_y\cdot v_W + v_z\cdot w_W \\ w_x\cdot(V_a + u_W) + w_y\cdot v_W + w_z\cdot w_W \end{bmatrix} \tag{6}
$$

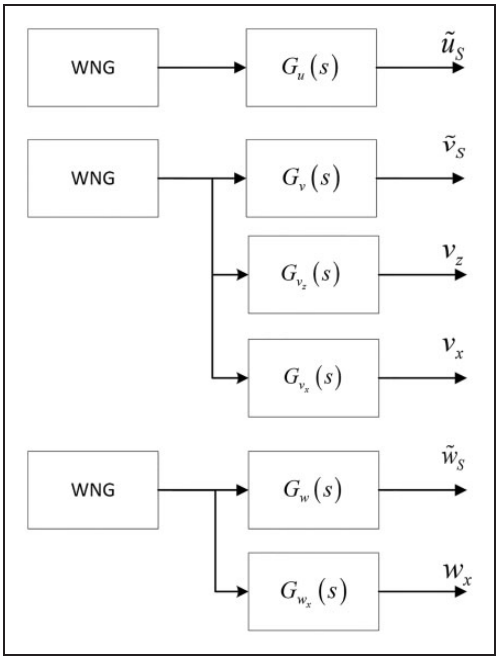

Figure 2. Dryden wind field computational structure.

where $\boldsymbol{V}_W = \boldsymbol{V}_G + \boldsymbol{V}_S$ represents the total wind field disturbance vector in hypersonic motion.

The transfer functions are equipped with first-order and second-order filters just as follows. The gains and time constants are functions of turbulence scale, intensity, airspeed, and wing span. Detailed information can be searched from Johnson.[11]

$$
\begin{aligned}
&G_u(s) = \frac{K_u}{T_u s + 1}, \quad G_v(s) = \frac{K_v}{T_v s + 1},\\
&G_w(s) = \frac{K_w}{T_w s + 1}\\
&G_{v_x}(s) = \frac{K_{vx}}{(T_v s + 1)(T_{vx} s + 1)}, \quad G_{v_z}(s) = \frac{K_{vz}}{(T_{vz} s + 1)}\\
&G_{w_x}(s) = \frac{K_{wx}}{(T_w s + 1)(T_{wx} s + 1)}
\end{aligned}
\tag{7}
$$

Wind field turbulences mainly affect the airspeed and aerodynamic angles of reentry vehicles.[28] According to the frame transformation, some compensation is added into the motion equations.

$$
\begin{aligned}
\dot{V}_a &= \frac{1}{M}(-D - Mg\sin\gamma) - \dot{u}_W\cos\gamma\cos\chi - \dot{v}_W\cos\gamma\sin\chi + \dot{w}_W\sin\gamma\\
\dot{\chi} &= \frac{1}{MV_a\cos\gamma}(Y + Mg\sin\mu\cos\gamma) - \frac{1}{V_a\cos\gamma}\big[\dot{u}_W(\sin\mu\sin\gamma\cos\chi\\
&\quad + \cos\mu\sin\chi) + \dot{v}_W(\sin\mu\sin\gamma\sin\chi + \cos\mu\cos\chi) + \dot{w}_W\sin\mu\cos\gamma\big]\\
\dot{\gamma} &= \frac{1}{MV_a}(L - Mg\cos\mu\cos\gamma) + \frac{1}{V_a}\big[\dot{u}_W(\cos\mu\sin\gamma\cos\chi + \sin\mu\sin\chi)\\
&\quad + \dot{v}_W(\cos\mu\sin\gamma\sin\chi - \sin\mu\cos\chi) + \dot{w}_W\cos\mu\cos\gamma\big]\\
\dot{\alpha} &= q - \tan\beta(p\cos\alpha + r\sin\alpha) + \frac{1}{MV_a\cos\beta}(-L + Mg\cos\mu)\\
&\quad - \frac{1}{V_a\cos\beta}\big[\dot{u}_W(\cos\mu\sin\gamma\cos\chi + \sin\mu\sin\chi)\\
&\quad + \dot{v}_W(\cos\mu\sin\gamma\sin\chi - \sin\mu\cos\chi) + \dot{w}_W\cos\mu\cos\gamma\big]\\
\dot{\beta} &= -r\cos\alpha + p\sin\alpha + \frac{1}{MV_a}(Y\cos\beta + Mg\sin\mu)\\
&\quad - \frac{1}{V_a}\big[\dot{u}_W(\sin\mu\sin\gamma\cos\chi - \cos\mu\sin\chi) + \dot{v}_W(\sin\mu\sin\gamma\sin\chi + \cos\mu\cos\chi) + \dot{w}_W\sin\mu\cos\gamma\big]\\
\dot{\mu} &= \sec\beta(p\cos\alpha + r\sin\alpha) + \frac{L}{MV_a}\tan\beta - \frac{g}{V_a}\tan\beta\cos\mu\\
&\quad + \frac{\tan\beta}{V_a}(\dot{u}_W\cos\mu\sin\gamma\cos\chi + \dot{v}_W\cos\mu\sin\gamma\sin\chi + \dot{w}_W\cos\mu\cos\gamma)\\
&\quad + \frac{\tan\gamma}{V_a}(\dot{u}_W\sin\mu\sin\gamma\cos\chi + \dot{v}_W\sin\mu\sin\gamma\sin\chi + \dot{w}_W\sin\mu\cos\gamma)
\end{aligned}
\tag{8}
$$

To obtain the output data for parameter identification, the input deflections (δ_e, δ_a, δ_r) are given as a standard 3-2-1-1 format (equation (9)).[22] In terms of empirical experiences, the control deflections are constrained within the range -10° to 10°.

$$
\delta = \begin{cases} a & , t \in (0, t_1)\\ -a & , t \in (t_1, t_2)\\ a & , t \in (t_2, t_3)\\ -a & , t \in (t_3, t_4)\\ 0 & , t \in (t_4, \infty) \end{cases}, \qquad a \in [-10^\circ, 10^\circ] \tag{9}
$$

Levy flight-based pigeon-inspired optimization

As a new swarm intelligence optimizer, PIO is an effective tool for optimal searching. PIO imitates the process of homing pigeons searching paths and provides a wider search space than other homogenous methods. In this section, we will introduce the computation process of basic PIO and propose a novel swarm intelligence optimizer based on this algorithm. Levy flight characteristics are implemented to improve the searching ability and overcome the limitation of local searching.

Procedure of basic PIO

Basic PIO is composed of two-stage operators. The first is the map and compass operator and the other is the landmark operator.[29] Map and compass operator

is inspired by the nature that pigeons use the sun and magnetic field as orientation sensors at initial flight. Assume X_i and V_i as the position and velocity of pigeon I, and X_g as the global best position of pigeon swarms, then this operator is described as

$$\begin{aligned} V_i(t) &= V_i(t-1)\cdot e^{-Rt} + rand\cdot\big(X_g - X_i(t-1)\big)\\ X_i(t) &= X_i(t-1) + V_i(t) \end{aligned} \tag{10}$$

where R defines the map and compass factor and *rand* is subject to the uniform distribution between 0 and 1.

Landmark operator manifests the landmark effects on the pigeons' flight. At this stage, half pigeons with inferior qualities tend to follow the superior ones. Meanwhile the half elite pigeons are likely to search paths in terms of the landmark X_c. Assume N_p is the swarm size of superior pigeons, so the landmark operator is given by

$$\begin{aligned} N_p(t) &= \frac{N_p(t-1)}{2}\\ X_c(t) &= \frac{\sum X_i(t-1)\cdot f_{\text{cost}}(X_i(t-1))}{N_p(t)\sum f_{\text{cost}}(X_i(t-1))}\\ X_i(t) &= X_i(t-1) + rand\cdot(X_c(t) - X_i(t-1)) \end{aligned} \tag{11}$$

where f_{cost} is a cost evaluation function. In this paper, we assume the parameter identification as a minimum value problem and adopt $f_{\text{cost}} = 1/(fit+\varepsilon)$. *fit* is the fitness function with regard to the identification issue, and ε is a constant small enough to ensure the feasibility.

Levy flight-based PIO

Although basic PIO performs well in some aspects, some flaws inherent are expected to be revised. For example, the search space for optima can be extended.[24–26] In this paper we propose a novel and efficient Levy flight-based pigeon-inspired optimization (LFPIO) to execute the model identification for the reentry vehicle.

LFPIO replaces the original operators of basic PIO with revised ones. Firstly we prefer to introduce the Levy flight theory to modify the first operator. Levy flight has been demonstrated that it is one of the best random walk models where the step lengths have a probability distribution that is heavy-tailed.[32] That is, in the process of flight, the step lengths are subject to Levy distribution.[33,34] When exploring a large-scale space, Levy flight is more available than other empirical motions because the variance of Levy distribution increases more rapidly. Hence during Levy flight, pigeons prefer to fly within a wider area by a faster speed. This mechanism can both extend the searching space and improve the convergence speed. Hence, we adopt the Levy flight search operator at the initial stage instead of the original map and compass operator. We use Mantegna's algorithm[35] to implement this operator.

$$\begin{aligned} s &= \frac{\lambda}{|\theta|^{1/\eta}},\quad \lambda\sim \mathrm{N}\big(0,\sigma_\lambda^2\big),\quad \theta\sim \mathrm{N}\big(0,\sigma_\theta^2\big),\quad \eta = 1.5\\ \sigma_\lambda &= \left(\frac{\Gamma(1+\eta)\sin\left(\frac{\pi\eta}{2}\right)}{\Gamma\left(\frac{1+\eta}{2}\right)\eta\cdot 2^{(\eta-1)/2}}\right)^{1/\eta},\quad \sigma_\theta = 1\\ X_p &= X_i(t-1) + s\cdot randn\cdot\big(X_i(t-1) - X_{\mathrm{g}}\big) \end{aligned} \tag{12}$$

where s is the step length of Levy flight, and *randn* is subject to the standard normal distribution. σ_λ and σ_θ are variances of corresponding normal distribution. In order to guarantee the convergence, the elite selection strategy is utilized as follows

$$X_i(t) = \begin{cases} X_p, & fit\big(X_p\big) < fit(X_i(t-1))\\ X_i(t-1), & fit\big(X_p\big) \geqslant fit(X_i(t-1)) \end{cases} \tag{13}$$

Moreover, although the landmark operator of basic PIO can accelerate the convergence speed, it easily leads to the prematurity and is constrained to local optima. Therefore, in order to increase the probability of global optima searching, we adopt the adaptive *Logsig* function[36] to adjust the step length and alleviate the convergence speed. Meanwhile, the renewable strategy is also suitable for each pigeon's dimensional update to jump out of local optima and avoid the prematurity. The revised landmark operator is presented as follows

$$\begin{aligned} &Step = Logsig\left(\frac{N_{\text{cm}}\cdot\zeta - t}{k}\right)\\ &\text{for each dimension } j \text{ of pigeon } i:\\ &X_i^j(t) = X_i^j(t-1) + Step\cdot randn\cdot\left(X_g^j - X_i^j(t-1)\right) \end{aligned} \tag{14}$$

where ζ and k are the adaptive parameters of *Logsig* function, which decide the convergence speed, and N_{cm} is the maximum iteration number.

Complexity analysis on PIO and LFPIO

The computational complexity of PIO and LFPIO is easily obtained from the mathematical expressions. Define the generation size N_p of each period, the dimensional size D_s of each pigeon and the computational load of fitness model L_f, the complexity of map and compass operator in basic PIO per period is $O((L_f + D_s)N_p)$ as we use equation (10) to update each pigeon's solution and conduct dimensional

judgment on solution boundaries. Likewise, we can obtain the complexity of the landmark operator in a period as $O(N_p \log N_p + D_s \log N_p + L_f \log N_p)$ from equation (11) due to the half swarm compression of each period and the quick sort algorithm used to compute the superior half generations. Assume the number of total iteration as N_c, we can sum up and give the computational complexity of basic PIO as $O(N_c(N_p D_s + N_p L_f + N_p \log N_p))$.

As for LFPIO, the computational load of Levy flight search operator is the same as the map and compass operator. However, the revised landmark operator is more sophisticated due to the dimensional update strategy in equation (14). This scheme could avoid the premature of local optima but increase the complexity because we must compute the fitness model with regard to each pigeon's dimension. Hence, the time complexity of the revised landmark operator is $O(N_p D_s L_f)$. Then we can get the total computational load of LFPIO as $O(N_c N_p D_s L_f)$.

Parameter identification for reentry vehicle via LFPIO

Small period (1.5 s) is concerned in this paper due to the Winged-Cone aerodynamic parameters are time-variant in long duration. Before the identification, the fitness function must be confirmed. To simplify this problem, the weighted accumulation of estimation errors in constant period is selected

$$J = \sum_{i=1}^{\tau} \int_{t_0}^{t_1} w_i (\hat{x}_i - x_i)^2 \mathrm{d}t, \quad t_1 - t_0 = T \tag{15}$$

where $\hat{x}_i$ and x_i are the identified outputs and actual outputs of the reentry system. T represents the identification period and $\tau = 10$ denotes the state number of reentry motion (9 state variables in equation (1) as well as altitude). w_i denotes the weight coefficient used to evaluate the importance of each state.

During one identification period, the Winged-Cone model with initial parameter groups is used. To evaluate the effects of wind shears, we plus some normal disturbances with certain intensity (e.g. Gauss white noises) into the preset model. Given the initial states and actual inputs at each period, we can obtain the estimated outputs through the preset model. Then, we can compute the fitness values in terms of the deviation between the actual and estimated outputs. The identification algorithm will evolve and screen out the elite parameter groups according to the fitness values. Hence, the identified aerodynamic parameters are recognized as the parameter groups with best fitness values. The detailed structure flow of this identification system is shown in Figure 3.

As for LFPIO, detailed procedure is described as the following steps and can be summarized in Figure 4. Besides we give the ranges of identified parameters listed in Table 2.

Step 1: Set the step size h equal to the sampling period and confirm the input format and identification period T.

Step 2: Initialize parameters of LFPIO, such as search space dimension D_s, maximum iteration N_{cm}, pigeon population size N_p and other relative parameters ζ and k.

Step 3: Each pigeon is equipped with a random position (a group of preset identified parameters) and substituted into the preset model. Then, we can obtain the estimated outputs and corresponding fitness values. Compare the fitness values and find the current best position.

Step 4: Update each pigeon's position with the Levy flight search operator, then substitute to the

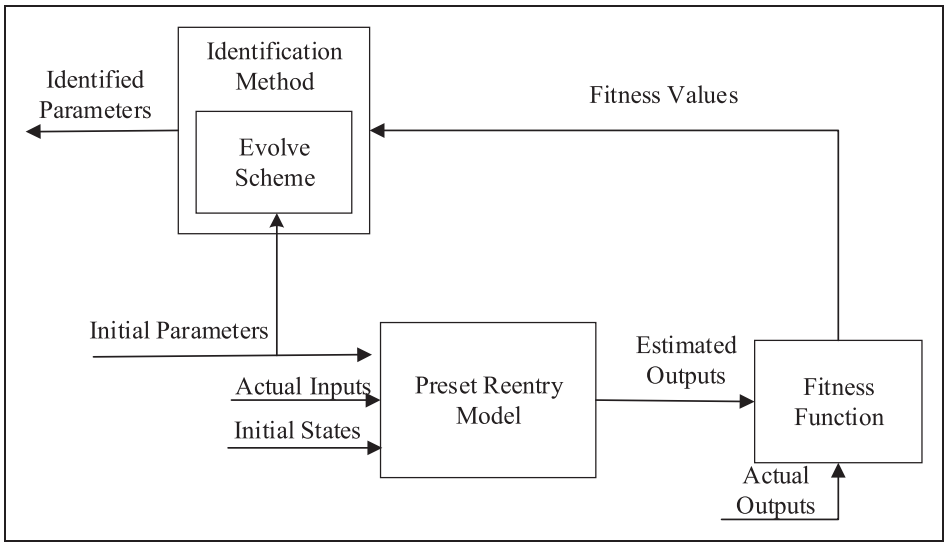

Figure 3. Structure of reentry identification system in a period.

model and obtain the new fitness values and best position.

Step 5: Using the revised landmark operator to avoid premature and improve the precision of global optima. Then update the relative variables.

Step 6: If the iteration number N_c is greater than maximum iteration N_{cm}, stop and output results. If not, go to Step 4.

Comparative results and analysis on LFPIO and other approaches

In this section, comparative experiments with other homogenous methods are conducted. Besides, the wind field turbulences at normal and strong level are also considered. The step time h is set as 0.03 s in this test and the number of data point in each identification period is 50. According to Table 2, the search space dimension of each pigeon D_s is 16. With regard to LFPIO, the swarm size of pigeons N_p is 50 and the maximum iteration N_{cm} is also 50. In accordance with test experiences, the parameters ζ and k in revised landmark operator are configured as 0.5 and 15. Because the aerodynamic angles are more critical for aerodynamic stability than angular rates in the reentry phase, the weights in fitness function are listed as in Table 3.

Other homogenous methods such as differential evolution (DE) and basic PIO algorithm are both implemented with the same values of common initial coefficients as LFPIO and two ranks of wind turbulences are also considered. For the normal rank, winds with maximum gust of 150 m/s, average wind shear of 100 m/s, and Gauss white noises with 20 dB intensity of the turbulence vector are involved. Mean fitness curves of different algorithms among 50 tests are shown in Figure 5. For the strong rank, winds with maximum gust of 240 m/s, average wind shear of 160 m/s, and Gauss white noises with 40 dB intensity are added to the reentry model. Comparative results of some critical states under the two rank winds are shown in Figures 6 and 7 and the best fitness values of various algorithms in two experiments are presented in Table 4. The expected states among the identification results represent the actual outputs of reentry vehicle.

The curves and fitness values shown in Figures 5 to 7 demonstrate that our proposed LFPIO could find out more accurate identification parameters than other applied algorithms in despite of the fitness curves or estimation results. Besides, the results in Table 4 indicate that although strong winds have a

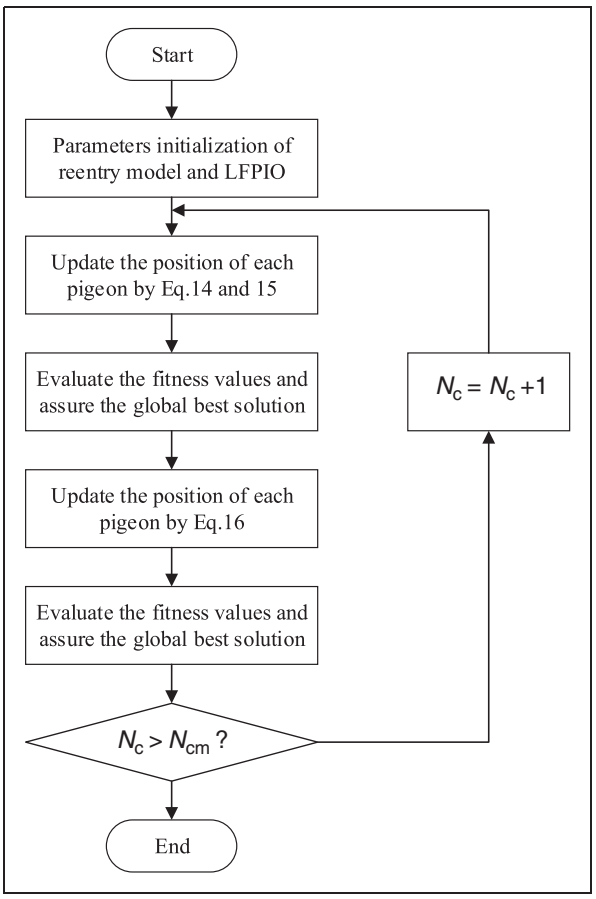

Figure 4. Flowchart of reentry identification via LFPIO.

Table 3. Weights of the fitness function in identification methods.

w_1	w_2	w_3	w_4	w_5
0.06	0.005	0.005	0.3	0.15
w_6	w_7	w_8	w_9	w_{10}
0.15	0.1	0.1	0.1	0.03

Table 2. Range list of identified parameters.

a_{11}	a_{12}	a_{13}	a_{21}	a_{22}	a_{23}	a_{31}	a_{32}
[−1e − 1, 1e − 1]	[−1e − 1, 1e − 1]	[−1e − 1, 1e − 1]	[−1e − 1, 1e − 1]	[−1e − 1, 1e − 1]	[−1e − 2, 1e − 2]	[−1, 1]	[−1e − 2, 1e − 2]
a_{41}	a_{42}	a_{43}	a_{51}	a_{52}	a_{53}	a_{61}	a_{62}
[−1, 1]	[−1e − 1, 1e − 1]	[−1e − 3, 1e − 3]	[−1e − 1, 1e − 1]	[−1e − 2, 1e − 2]	[−1e − 2, 1e − 2]	[−1e − 3, 1e − 3]	[−1e − 1, 1e − 1]

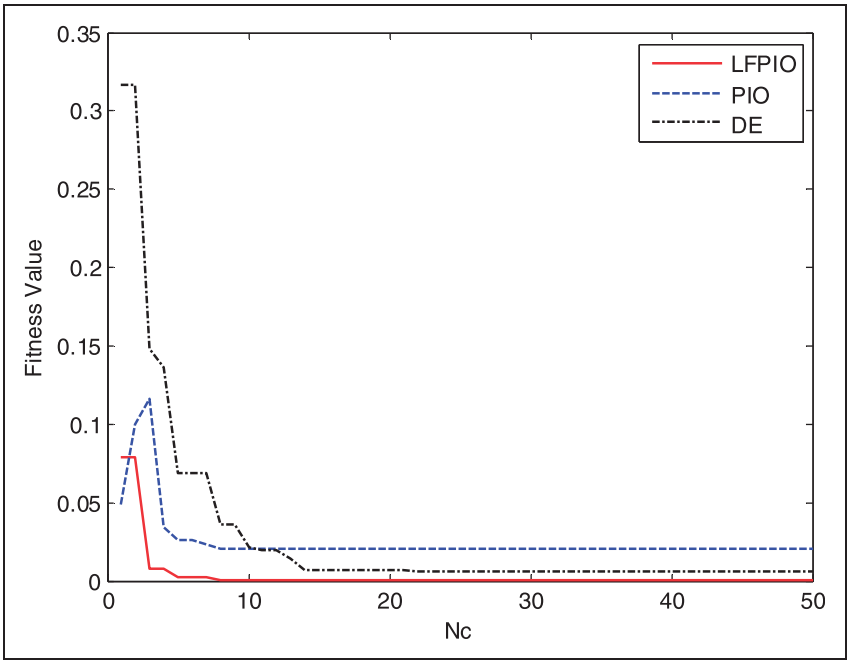

Figure 5. Fitness curves for various identification methods within normal winds.
LFPIO: Levy flight-based pigeon-inspired optimization; PIO: pigeon-inspired optimization; DE: differential evolution.

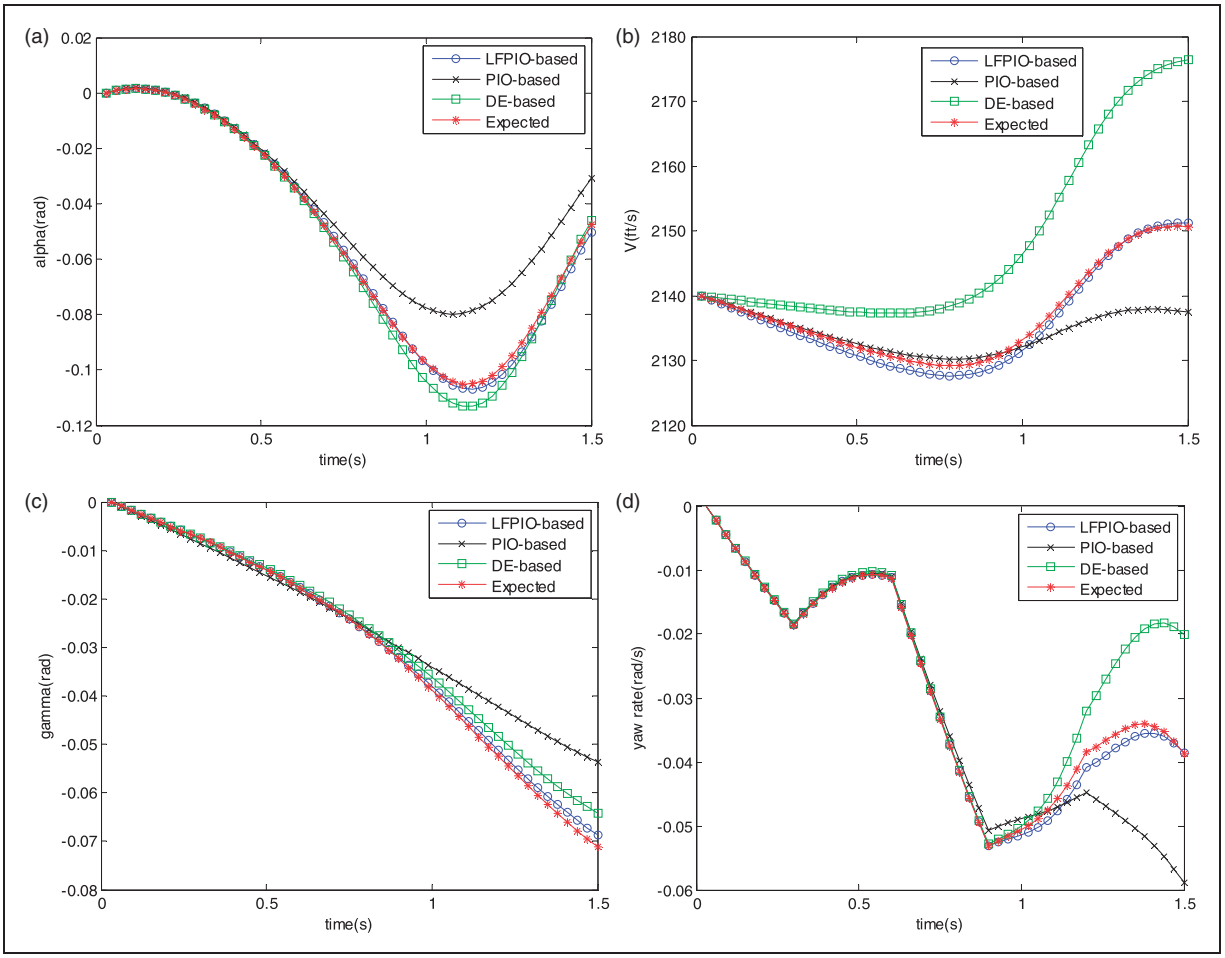

Figure 6. Comparative results for reentry vehicle identification within normal winds: (a) identified results for attack angle α; (b) identified results for airspeed V_a; (c) identified results for bank angle γ; (d) identified results for yaw rate r.
LFPIO: Levy flight-based pigeon-inspired optimization; PIO: pigeon-inspired optimization; DE: differential evolution.

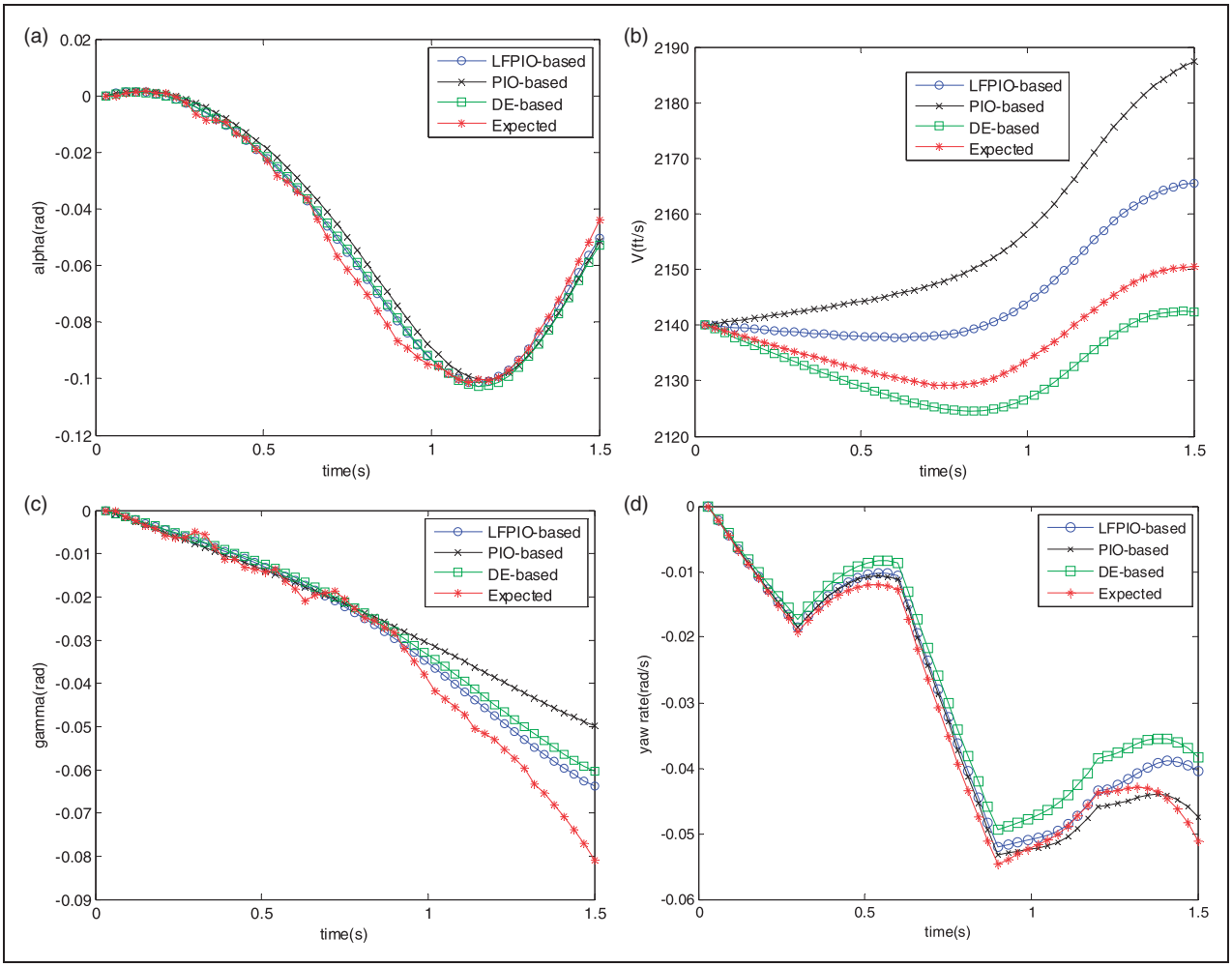

Figure 7. Comparative results for reentry vehicle identification within strong winds: (a) identified results for attack angle α; (b) identified results for airspeed V_a; (c) identified results for bank angle γ; (d) identified results for yaw rate r.
LFPIO: Levy flight-based pigeon-inspired optimization; PIO: pigeon-inspired optimization; DE: differential evolution.

Table 4. The best fitness values of various algorithms in two rank experiments.

	LFPIO	PIO	DE
Normal winds turbulences	4.3893e − 004	0.0102	0.0056
Strong winds turbulences	0.0012	0.0159	0.0078

LFPIO: Levy flight-based pigeon-inspired optimization; PIO: pigeon-inspired optimization; DE: differential evolution.

few effects on the identification performance, LFPIO is still more reliable than other homogenous methods in complicated environments. It is assumed that the reasons for the exact accuracy of LFPIO include two aspects. On the one hand, the introduced Levy flight mechanism could extend the search space and each solution is prone to investigate in a wider feasible area. Moreover, the step length of Levy distribution is larger than other typical distributions, which guarantees the balance between the convergence speed and search precision. On the other hand, the adaptive *Logsig* function in the revised landmark operator smoothes the trend of convergence in the shape of hyperbolic descending form instead of linearity. Meantime, the dimensional update scheme provides a more comprehensive global searching ability by evaluating dimensional fitness and increasing the time complexity. Hence, the revised landmark operator could avoid the premature and improve the accuracy of global optima no matter how much the stress magnitude of wind turbulences, although it is easily subject to longer computation time. Hence, it is concluded that our proposed LFPIO is an efficient offline identification method for parameter estimation of reentry vehicles.

Conclusions

This paper focuses on the solution of offline identification problem for a hypersonic reentry vehicle and proposes a novel bio-inspired method for the issue. A complete nonlinear Winged-Cone model with wind field disturbances is introduced first, and the relevant aerodynamic coefficients for this model are assigned as five-order polynomials of Mach number,

attack angle, and control deflections. Hence, the objective for reentry identification is decision of parameters in the Winged-Cone polynomials. Then a novel LFPIO algorithm is developed to cope with the identification issue. This bio-inspired algorithm derives from PIO, and in order to improve the precision of each solution, two original operators of basic PIO are replaced. For the first operator, Levy flight mechanism is added to extend the search space and balance the convergence speed. For the other one, an adaptive function with smoothly convergence gradient is used to slow down the trend of local optima and the dimensional update scheme is applied to provide searching accuracy, thus improving the probability of finding out global optima. Through comparative experiments with other homogenous methods, LFPIO could provide more precise result without convergence speed descending under different environments despite its high computational load.

Hence, it is concluded that our proposed LFPIO could serve as an effective algorithm for offline reentry identification and facilitate the controller design or other research issues of reentry vehicles. In the future, it is expected that LFPIO could be applied and developed in other crucial engineering and theoretical aspects. What's more, simple and feasible aerodynamic models are expected to engage in the study of reentry vehicles.

Declaration of Conflicting Interests

The author(s) declared no potential conflicts of interest with respect to the research, authorship, and/or publication of this article.

Funding

The author(s) disclosed receipt of the following financial support for the research, authorship, and/or publication of this article: This work was partially supported by National Natural Science Foundation of China (grant #61673327 and #61333006), and Aeronautical Foundation of China (grant #2015ZA51013).

References

1. Liu GF, Li DC, Xiang JW, et al. Design, modeling and analysis of a sharp-edge hypersonic stealthy re-entry vehicle. *Procedia Eng* 2015; 99: 163–167.
2. Gao JQ, Dou LQ and Su PH. Multi-model switching control of hypersonic vehicle with variable scramjet inlet based on adaptive neural network. In: *12th world congress on intelligent control and automation*, Guilin, China, 12–15 June 2016, pp.1714–1719.
3. An H, Liu JX, Wang CH, et al. Approximate back-stepping fault-tolerant control of the flexible air-breathing hypersonic vehicle. *IEEE/ASME Trans Mechatron* 2016; 21: 1680–1691.
4. Wang Z, Wu Z and Du YJ. Robust adaptive backstepping control for reentry reusable launch vehicles. *Acta Astronaut* 2016; 126: 258–264.
5. Wu HN, Liu ZY and Guo L. Robust L_∞-Gain fuzzy disturbance observer-based control design with adaptive bounding for a hypersonic vehicle. *IEEE Trans Fuzzy Syst* 2014; 22: 1401–1412.
6. Oppenheimer M, Skujins T, Doman DB, et al. A flexible hypersonic vehicle model developed with Piston Theory. In: *AIAA atmospheric flight mechanics conference and exhibit*, Hilton Head, SC, USA, 20–23 August 2007, AIAA 2007-6396.
7. Shaughnessy JD, Pinckney SZ, McMinn JD, et al. Hypersonic vehicle simulation model: Winged-Cone configuration. Report, Langley Research Center, NASA-TM-102610, 1 November 1990.
8. Keshmiri S, Colgren R and Mirmirani M. Development of an aerodynamic database for a generic hypersonic air vehicle. In: *AIAA guidance, navigation and control conference and exhibit*, San Francisco, CA, USA, 15–18 August 2005, AIAA-2005-6257.
9. Klock RJ and Cesnik CE. Aerothermoelastic reduced-order model of a hypersonic vehicle. In: *AIAA atmospheric flight mechanics conference*, Dallas, TX, USA, 22–26 June 2015, AIAA-2015-2711.
10. Liang W and Song F. Modelling flow transition in a hypersonic boundary layer with Reynolds-averaged Navier-Stokes approach. *Sci China Ser G* 2009; 52: 768–774.
11. Johnson DL. Terrestrial environment (climatic) criteria guidelines for use in aerospace vehicle development, 2008 Revision. Report, Marshall Space Flight Center, NASA-TM-2008-215633, 2008.
12. Du YL, Wu QX, Jiang CS, et al. Adaptive functional link network control of near-space vehicles with dynamical uncertainties. *J Syst Eng Electron* 2010; 21: 868–876.
13. Du YL, Wu QX, Jiang CS, et al. Adaptive recurrent-functional-link-network control for hypersonic vehicles with atmospheric disturbances. *Sci China Inf Sci* 2011; 54: 482–497.
14. Vitale A, Corraro F, Bernard M, et al. Identification of the transonic aerodynamic model for a re-entry vehicle. In: *Proceedings of the 15th IFAC symposium on system identification*, Saint-Malo, France, 6–8 July 2009, pp.1211–1216.
15. Hu CF and Liu QZ. Online identification for hypersonic vehicle using recursive maximum likelihood method based on interior-point algorithm. In: *25th Chinese control and decision conference*, Guiyang, China, 25–27 May 2013, pp.1862–1867.
16. Silveira G, Kuga HK and Oliveira EJ. Application of extended Kalman filter in estimation of reentry trajectories. In: *International congress of mechanical engineering*, Ribeirao Preto, Brazil, 3–7 November 2013, pp.3618–3627.
17. Yuan XX, Chen JQ and Wang WZ. Pitching dynamic stability computation for plane nose reentry vehicle and flow mechanism analysis. *Acta Aerodyn Sin* 2007; 25: 300–305.
18. Qiu HX, Wei C, Dou R, et al. Fully autonomous flying: From collective motion in bird flocks to unmanned aerial vehicle autonomous swarms. *Sci China Inf Sci* 2015; 58: 1–3.
19. Zhong WJ, Wang JS, Ji WJ, et al. The attitude estimation of three-axis stabilized satellites using hybrid particle swarm optimization combined with radar cross section precise prediction. *Proc IMechE, Part G: J Aerospace Engineering* 2016; 230: 713–725.

20. Erdbrink CD and Krzhizhanovskaya VV. Differential evolution for system identification of self-excited vibrations. *J Comput Sci* 2015; 10: 360–369.
21. Gao F, Fei FX, Xu Q, et al. A novel artificial bee colony algorithm with space contraction for unknown parameters identification and time-delays of chaotic systems. *Appl Math Comput* 2012; 219: 552–568.
22. Li ST and Duan HB. Artificial bee colony approach to online parameters identification for hypersonic vehicle. *Scient Sin Informat* 2012; 42: 1350–1363.
23. Li C and Duan HB. Target detection approach for UAVs via improved pigeon-inspired optimization and edge potential function. *Aerosp Sci Technol* 2014; 29: 352–360.
24. Zhang B and Duan HB. Three-dimensional path planning for uninhabited combat aerial vehicle based on predator-prey pigeon-inspired optimization in dynamic environment. *IEEE Trans Comput Biol Bioinform* 2015; 14: 97–107.
25. Duan HB and Wang XH. Echo state networks with orthogonal pigeon-inspired optimization for image restoration. *IEEE Trans Neural Netw Learn Syst* 2015; 27: 2413–2425.
26. Zhang SJ and Duan HB. Gaussian pigeon-inspired optimization approach to orbital spacecraft formation reconfiguration. *Chin J Aeronaut* 2015; 28: 200–205.
27. Xue Q and Duan HB. Robust attitude control for reusable launch vehicles based on fractional calculus and pigeon-inspired optimization. *IEEE/CAA J Automat Sin* 2017; 4: 89–97.
28. Deng YM and Duan HB. Control parameter design for automatic carrier landing system via pigeon-inspired optimization. *Nonlin Dyn* 2016; 85: 97–106.
29. Duan HB and Qiao PX. Pigeon-inspired optimization: a new swarm intelligence optimizer for air robot path planning. *Int J Intell Comput Cybernet* 2014; 7: 24–37.
30. Cai GH, Song JM and Chen XX. Control system design for hypersonic reentry vehicle driven by aerosurfaces and reaction control system. *Proc IMechE, Part G: J Aerospace Engineering* 2015; 229: 1575–1587.
31. Du YL, Lu YP, Wu QX, et al. Modeling of thrust misalignment and wind disturbances for air-breathing hypersonic vehicles. In: *Proceedings of international conference on modeling, identification and control*, Wuhan, China, 24–26 June 2012, pp.345–352.
32. Barthelemy P, Bertolotti J and Wiersma DS. A Levy flight for light. *Nature* 2008; 453: 495–498.
33. Eliazar I. A geometric theory for Levy distributions. *Ann Phys* 2014; 347: 261–286.
34. Aydogdu I, Akin A and Saka MP. Design optimization of real world steel space frames using artificial bee colony algorithm with Levy flight distribution. *Adv Eng Softw* 2016; 92: 1–14.
35. Mantegna RN and Stanley HE. Stochastic process with ultraslow convergence to a Gaussian: The truncated Levy flight. *Phys Rev Lett* 1994; 73: 2946–2949.
36. Tang L, Li T and Perng CS. *LogSig*: Generating system events from raw textual logs. In: *Proceedings of the 20th ACM conference on information & knowledge management*, Glasgow, UK, 24–28 October 2011, pp.785–794.